# Underlying causes of the improved storage properties of $TiMn_{1,5}$ by annealing treatment.

AUTHOR NAMES:
Simon $Arnal^{l}$ , $Anne\ Maynadier^{l}*$ , $Laetitia\ Laversenne^{2}$ , $David\ Chapelle^{l}$ .
AUTHOR ADDRESS:
<sup>1</sup> Université de Franche-Comté, CNRS, Institut FEMTO-ST, FCLAB, 25000 Besançon, France
<sup>2</sup> University Grenoble Alpes, CNRS, Grenoble INP, Institut Néel, 38000, Grenoble, France
KEYWORDS:
Solid State Hydrogen Storage;
Reversible hydrides;
TiMn <sub>1.5</sub> intermetallic compound;
Microstructural mechanism;
Metallurgical annealing;
Techniques for improving hydrogen storage properties.

#### **ABSTRACT**

The TiMn<sub>1.5</sub> intermetallic alloy in powder form is a good medium for the reversible storage of hydrogen in solid form. Since the 1980s, it has been known that optimizing its storage properties requires time-consuming and costly annealing at 1100°C for 20 hours. However, effects induced by heat treatment and the link between micro modification and macro functional properties are still not clearly established. The present work aims at bringing insights on the changes at the micro scale which can explain the observed improvement of hydrogen storage properties (capacity from 1.42wt%H to 1.75wt%H, lower transformation pressure and flattening of PCI plateau). The particles morphology and size, the phase-structural composition and microstructure were characterized by SEM microscopy, EDS and XRD techniques before and after annealing. During the treatment, the particles morphology drastically changes, gradually forming foamy, "coral-like" particles from grounded faceted particles, increasing the active surface. Inside the faceted particles, we observe a counter-intuitive increase of the amount of the TiMnα phase, known to poorly desorb hydrogen but acts as a catalyst during absorption process. EDS shows a Mn- enrichment of the Laves phase, while crystal lattice broadening measured by XRD is very slight. The Rietveld refinement on the still predominant C14 phase shows that the lattice strain decreases from 2,03.10 <sup>3</sup> to 8,3.10<sup>-4</sup> highlighting a relaxation phenomenon. Based on these observations, we conclude that the combination of these phenomena plays an essential role in the improvement of the storage capacity and pressure during the annealing process.

## INTRODUCTION:

For several decades, the development of renewable energy production solutions has been booming. By their very nature, these sources of energy have the major disadvantage of operating intermittently, constrained by environmental conditions, and out of phase with consumption. In order to meet the energy demand during peak consumption periods and to increase the profitability of the installations, it is necessary to store the daily, or even seasonal, production surpluses. Electricity surplus from solar and wind power plants can be stored over the long term by producing hydrogen through water electrolysis. Thereafter, several hydrogen storage technologies with different degrees of maturity are possible. Storage of hydrogen in liquid form, known as cryogenic storage, requires a low temperature maintenance (-252°C). This thermal regulation is energy consuming and induces evaporation problems [1]. Storage in compressed form is the most mature technology today, and the preferred choice for mobility applications. Type IV tanks, reinforced by carbon filament winding, can store di-hydrogen gas at pressure at 700 bars with a gravimetric hydrogen capacity around 5%wt; which makes this technology very competitive [2]. However, the management of safety at high pressure and its energy cost due to compression are limiting factors to the commercialization [3]. The last hydrogen storage technology, less mature but promising, is solid state storage based on metal hydrides. this is based on the reversible hydriding of certain intermetallic alloys at near-ambient temperatures (from 0 to 50°C) and pressures (between 1 to 50°C) bar). This storage technology has many advantages for stationary hydrogen storage facilities or for heavy mobility (construction equipment, public works, heavy industry, etc.). Despite a low gravimetric capacity (lower than 5wt% H), non-critical for stationary storage, the volumetric capacity is relevant (until 160kg H2/m3). Furthermore, the operating pressure is close to the atmospheric pressure. Above all, in these troubled times of competition for strategic resources and metals, some storage media are based on readily available and abundant metal components such as Ti, Fe and Ni. Moreover, these alloys can be regenerated by heat treatment or even easily recycled.

The intermetallic compounds of AB2 type are known for their good reversible storage capacities [4], [5]. Among them, Gamo et al studied the H-desorption of several Ti-Mn based binary alloys powders [6]. They highlight that, whereas the absorption capacity increases with the Ti contain, the desorption is optimal for a Ti proportion near 40%. The TiMn<sub>1.5</sub> give the best reversible storage capacity. Theoretically, the hydride induced structure is TiMn<sub>1.5</sub>H<sub>2.3</sub> leading to a storage saturation at H/M≈0.92. Gamo et al experimentally characterize the desorption capacity, plotting Pressure -Composition – Isothermal curves. The PCI curve of the as cast- as crushed powder at 20°C reveals a plateau at 0.75 MPa at 0.6 H/M a saturation around 0.8H/M and entrapped hydrogen amount around 0.15 H/M. The authors then propose an annealing heat treatment of 20 hours at 1100°C. The PCI curve of the treated powder shows a flatter plateau and most of all a significant improvement of the absorption and reversible desorption quantities: the saturation is slightly higher than 0.9 H/M for a residual trapped hydrogen amount lowered to 0.1 H/M. This simple heat treatment makes the TiMn<sub>1.5</sub> compound a good candidate for solid state storage technology at low pressure and temperature operating conditions. However, the metallurgical mechanisms leading to this improvement are not clearly elucidated in the paper. The authors merely hypothesize that the extent and the flattening of the plateau is dependent of the lattice constant and the organization of the present phases at the microstructure scale. Later, microstructural characteristics and their evolution during hydrogenation on TiMn<sub>1.5</sub> were studied by Singh et al [7] using XRD, TEM and Sievert'apparatus. Singh et al propose that TiMn<sub>1.5</sub> can be considered as TiMn<sub>2</sub>, with titanium atoms partially substituting manganese sites in a C14 Laves structure. As Mn has a larger atomic size than Ti, this distorts the lattice and enlarges the interstitial voids, facilitating hydrogen uptake. According to Singh *et al*, this model may be sufficient to explain why  $TiMn_{1.5}$  is the optimum alloy among TiMn<sub>2-x</sub> (x=0-1.25) alloys. However, the reasons of the correlation between improved

hydrogen storage properties and the annealing process are not yet clearly established whereas this heat treatment is often applied indiscriminately to many metal hydrides, without formal knowledge of the underlying mechanisms.

According to the phase diagram proposed by Khan et al. [8], reproduced in **Figure 1**, TiMn<sub>1.5</sub> is located in a two-phase domain with a structure called TiMnα (named TiMn1+x on the diagram) and a hexagonal structure TiMn<sub>2</sub> (Laves C14) of space group P63/mmc. The structure TiMnα is mentioned in some studies [6], [9], [10] but the crystallographic structure is undetermined.

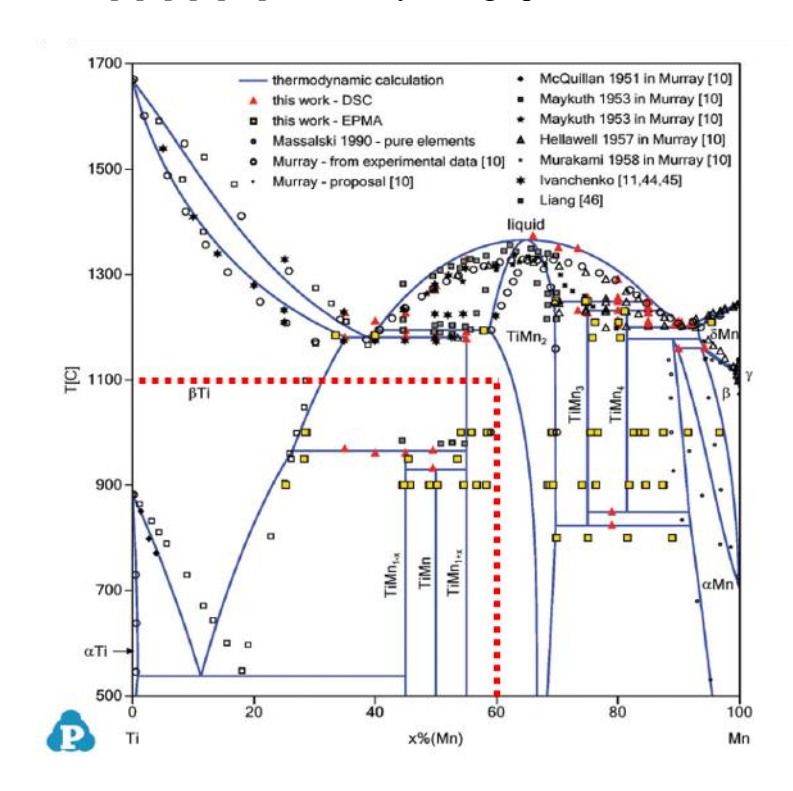


**Figure 1.** Thermodynamic calculation of the phase diagram of the Ti-Mn system suggested by A. U. Khan [8] (*Reproduced from [8] with permission from the PCCP Owner Societies*). The overprinted red doted lines enhance the TiMn<sub>1.5</sub> alloy and the 1100°C temperature.

To finally elucidate why the annealing prescribed by Gamo *et al.* in the 80's improves the storage properties of TiMn1.5, our objective is to discriminate the induced micro-scale mechanisms that can explain the changes in macroscopic storage behavior, *i.e.* here the increase in storage capacity

and the flattening of the absorption/desorption plateaus. The aims of the present study are firstly to validate the reproducibility of the Gamo annealing treatment and secondly to identify the modifications caused by the heat treatment that are responsible for the improved hydrogen storage. The physico-chemical and micromechanical phenomena involved in annealing are at the heart of this work. Mechanisms occurring during hydriding are not studied here. All results are based on a comparison between a raw industrial powder of TiMn.1.5 and two batches treated after annealing at 1100°C for 10h or 20h but before any exposure to hydrogen. In the first part of this article, we present the studied material and we detail the experimental techniques employed: volumetric methods in order to obtain the PCI curves, SEM electronic imaging, EDX quantification and structural analysis by XRD. The results derived from these experiments are then presented and analyzed in a second part, to gain insight into the effect of microstructural changes on hydrogen storage capacity.

## **EXPERIMENTAL SECTION:**

# Material and annealing heat treatment.

The TiMn<sub>1.5</sub> intermetallic alloy is industrially synthesized by melting 99.9% pure metals heated in an induction furnace controlled under an argon atmosphere. Once the metal is molten, it is poured into a copper crucible. The sample is maintained under argon gas until reaching a temperature of 300 to 400°C. The as cast alloy ingots is then crushed and ground with a blade mill to finally be sieved and stored as calibrated particles between 1 and 2 mm. The obtained powder is then thermally treated in our laboratory, at 1100°C during 10h for the first batch and 20 h for the second, under 1.2 bar argon atmosphere. In the following paragraphs, the different characterization techniques used to investigate the H-storage capacity, the chemical modifications, meso- and micro-structural changes, and the lattice transformations are detailed.

#### Characterization methods.

The absorption/desorption properties in isothermal condition are investigates thought the socalled PCI curves (Pressure-Composition-Isothermal diagram). The analyses are performed using the Sievert volumetric method on a IMI Hiden Isochema instrument. This method measures, in moles, the amount of hydrogen absorbed or desorbed by the intermetallic compound, for different equilibrium pressures at a given temperature (here 22°C) in a fixed dosing volume.

Powder particle morphology and size, as well as the microstructure inside the particles, were observed by scanning electron microscopy (SEM). The inner observations of the microstructure and the energy-dispersive X-ray spectroscopy (EDXS) analyses are made possible in SEM after the TiMn<sub>1.5</sub> powder has been embedded in *Graphite 617* conductive resin from LAMPLAN and then polished first with fine abrasive paper and then with colloidal silica solution. SEM observations are made with an APREO S SEM microscope in the cleanroom of MIMENTO plateform (micro-nano-technology center in Besançon F-25000 member of the French RENATECH network). The observations and analyses are performed under a voltage of 20kV, a current of 2nA and a vacuum of 10<sup>-6</sup> mbar. The granularity, i.e. the statistical analysis of the size distributions, of the powder particles is performed by image analysis using the ImageJ software [11]. The chemical species concentration profiles, inside the particles, are established from the average of 3 successive scans (50 points) with a dwell time per pixel of 1 second. The composition maps are realized by the average acquisition of 200 scans with an analysis time per pixel of 1 second to obtain a mapping resolution of 256x170 pixels.

The analysis of the microstructure is completed by X-Ray Diffraction (XRD) measurements to identify the actual phases present or the lattice distortion evolution. These measurements were

conducted at the Néel Institute in Grenoble, with a diffractometer *Bruker D8Endeavor* and a *LynxEye-XE* detector. The acquisition of the diffractograms is done by the Bragg Brentano method on a powder bed, with an emitting source CuK $\alpha$ 1 ( $\lambda_{\text{CuK}}$   $\alpha$ 1=1.540598 Å) for a duration of 4 hours.

## **RESULTS AND DISCUSSION:**

# H Absorption/Desorption properties from PCI curves.

In order to confirmed the effect of the heat treatment proposed by Gamo et al in [6] on the storage capacity improvement of the TiMn<sub>1.5</sub> alloy powder, Pressure-Composition-Isothermal (PCI) curves are built thanks to Sievert analyses. Figure 2 shows the PCI curves of TiMn<sub>1.5</sub> powder ascast and after a heat-treatment during 10h or 20h. As expected, the increase in maximum absorption capacity and flattening of the phase transformation plateau after annealing is notable. The characteristic parameters at 22°C (absorption capacity at 100bar, equilibrium pressures), allowing to quantify this improvement are listed in Table 1. Absorption and desorption pressure are determined as the pressure in the middle of the transformation plateau, based on three tangent straight lines. The PCI curves after a treatment of 10h or 20h are almost superimposed. In both cases, the thermal treatment induces a capacity increase from 1.42%wtH to 1.75%wtH at 100bar, i.e. a 23% increase. Phase transformation of the heat-treated powder starts distinctly for a pressure close to 15 bar and ends at 40 bar, while the as-cast powder transitions are not identifiable and the formation of the  $\beta$  phase does not seem to be fully completed at 100 bar. Due to these observations and in order to save energy and time, as the storage properties are identical after a 10h or 20h annealing, in the following the characterizations will be carried out on powder annealed for 10h at 1100°C.

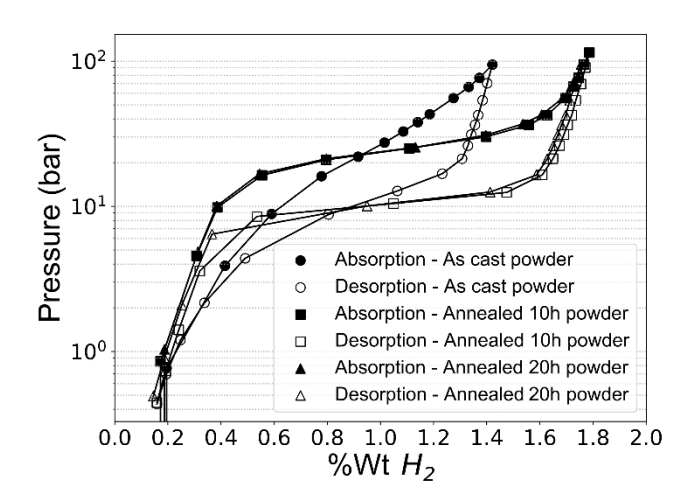


**Figure 2.** Pressure-Composition-Isothermal diagram obtained at 22°C of the as cast powder, the 10h annealed powder and 20h annealed powder of TiMn<sub>1.5</sub>

Powder	100 bar capacity (%wt H)	Absorption pressure (bar)	Desorption pressure (bar)	
As cast	1.42	30	12	
Annealed	1.75	25	10	

**Table 1.** Absorption/desorption properties measured by Sievert apparatus at 22°C for the as cast, the 10h annealed TiMn<sub>1.5</sub> powder

# Powder morphology and inner microstructure.

The SEM observations of two batches (one of raw industrial TiMn1.5 powder and the other of powder heat-treated at 1100°C for 10 hours, both before hydrogenation) revealed two types of particle morphologies, shown in **Figure 3**. The first type, corresponding to the major part of the particles before treatment, is commonly found after grinding with dense and faceted particles,

Figure 3(a). The second type corresponds to particles that appear porous or even foamy and crumbly, with an appearance that evokes coral, Figure 3(b).

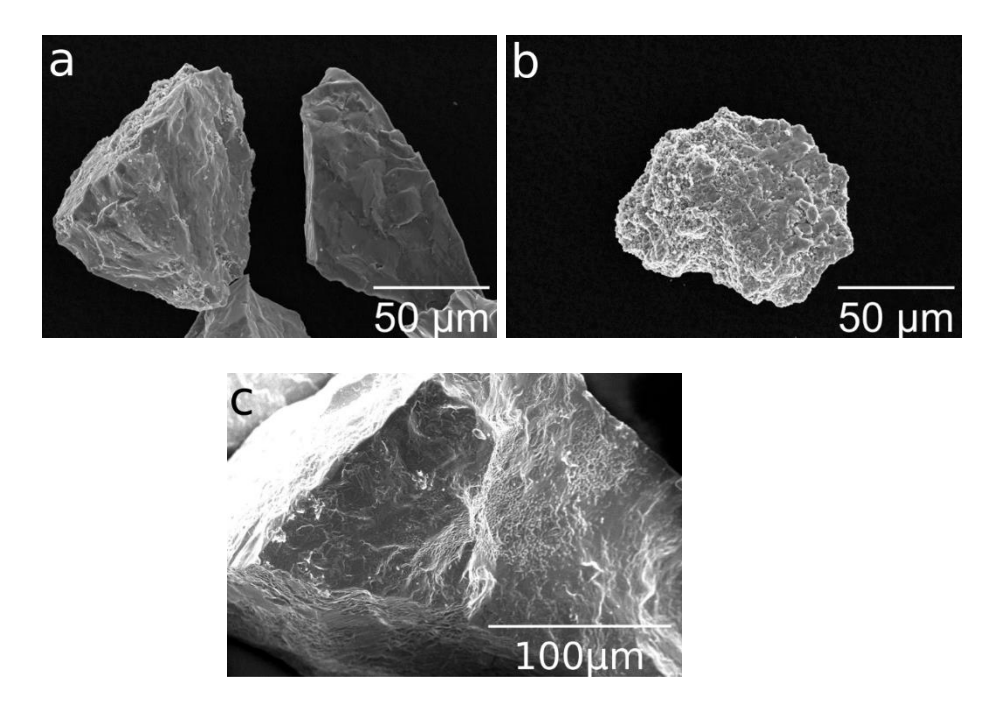


**Figure 3.** SEM pictures: (a) dense faceted particles; (b) foamy, coral-like, particles whose occurrence increases after heat treatment; (c) faceted particle with mixed zone

Moreover, a closer look at the dense faceted particles of the treated batch reveals the sparse presence of mixed zones on some surface: whitened and roughened areas **Figure 3(c)**. Statistical distribution analysis of the particles, based on SEM images with 150 particles before and 150 particles after treatment, but still before hydrogenation, shows a 20% increase in the number of coral-like particles after annealing. Moreover, whereas faceted particles represented 84% before treatment, they are only 14% after annealing: most particles seem to be in the process of being transformed. In addition, the average diameter decreases during the heat treatment from 75μm for the as cast powder to 51 μm for the annealed powder.

In what follows, we focus on the changes that may have taken place at the core of the particles. Particles are embedded in a conductive resin and polished in order to observe the inner microstructure. Contrasting areas of the back-scattered electron image in **Figure 4** reveal a heterogeneous microstructure. It shows grey domains of elongated shape in a white matrix. Additional measurements are performed to determine the composition and distribution in the particles core by EDS spectroscopy. **Figure 5(a)** is a composition map of the element Ti constructed by identification of the  $K\alpha_1$  lines of titanium. The bright areas are the richest in titanium. **Figure 5(b)** is a concentration profile of titanium and manganese measured on the same particle along the red dashed arrow drawn in **Figure 5(a)**.

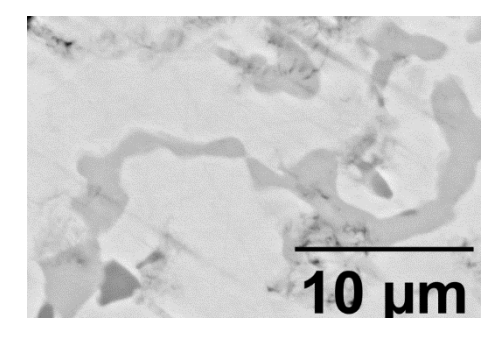
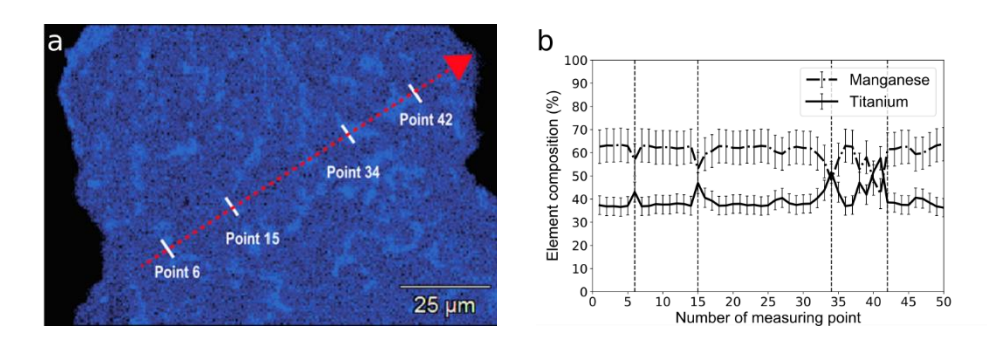


Figure 4. Back-scattered electron image of a faceted particle of as cast TiMn<sub>1.5</sub> powder

These two analyses show that inside the particles, the microstructure is heterogeneous. The composition profile, despite EDS measurement errors, suggests the presence of narrow domains of  $TiMn_{\alpha}$ , with composition close to 50%at. Mn and 50%at. Ti surrounding larger domains with composition varying from to 60%at. Mn and 40%at. Ti to 64%at of Mn and 36%Ti that can be identified as  $TiMn_{x,x=1.5...1.7}$ .



**Figure 5.** EDS analyses of polished particle of annealed TiMn<sub>1.5</sub> powder: (a) Composition map (Ti-richest areas are brighter); (b) Composition profile of Manganese and Titanium along the red dotted line.

In addition, the proportion of  $TiMn_{\alpha}$  phase in numerous particles is measured by image correlation method from the EDS maps, before and after heat treatment. Assuming that the volume distribution is the same as the surface distribution on these analysis maps, the volume proportion of  $TiMn_{\alpha}$  phase in the particles is 3% for the as cast powder, while it is 9% for the annealed powder.

A previous work of Yu Xinnan [12] highlights the formation of surface oxide in presence of poisoning gaseous and it leads to the manganese segregation on particles surface. In our case, the EDS analyses, (as shown in **Figure 5(a)**) do not allow to conclude to a significant segregation of titanium or manganese on the surface of the particles. The potential formation of oxide on the surface is not detected by EDS analysis. However, according to the image correlation analysis, the volume proportion of TiMnα phase increases between the as-cast and heat-treated state in the core of the particles. It is therefore reasonable to assume that intra-particle migration of Ti from TiMn<sub>1.5</sub> domains toward TiMnα domains is thermally activated by the heat-treatment, leading to the expansion of surface occupied by TiMnα. This internal segregation may be explained by the wide existence range of the Laves C<sub>14</sub> phase between TiMn<sub>1.25</sub> and TiMn<sub>2</sub> as per the Gamo study's [6].

# X-Ray Diffraction analyses.

The X-Ray-Diffraction analyses are shown in the **Figure 6** and **Figure 7**, respectively for the as-cast powder and the 10h annealed powder. A common reference of silicon is used to the TiMn<sub>1.5</sub> powder with a known lattice parameter for indexing purpose. Referring to the phase diagram [1] (**Figure 1**) and Ti-Mn alloys studies ([6],[7],[13]), the TiMn<sub>1.5</sub> compound has a Laves C<sub>14</sub> structure similar to TiMn<sub>2</sub>.

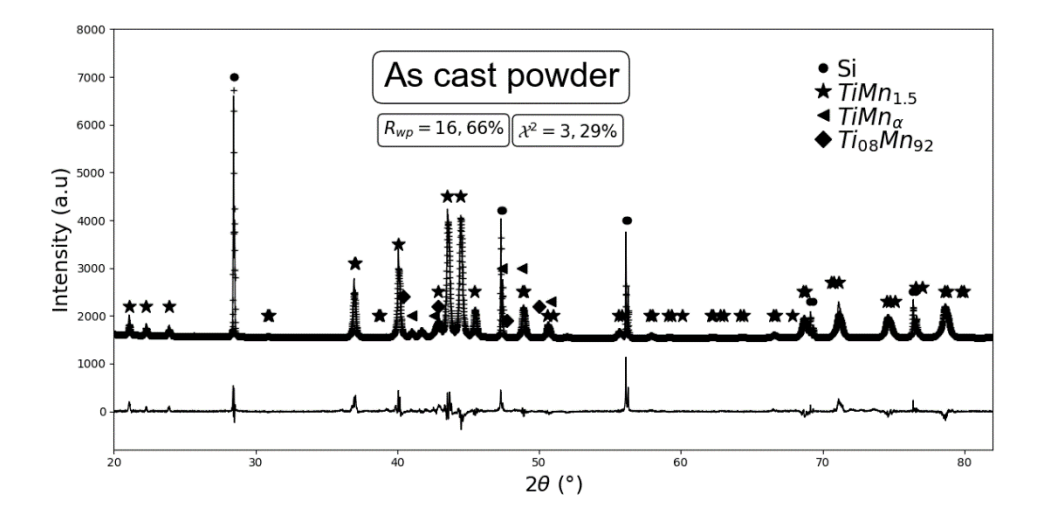


**Figure 6.** Rietveld refinement (line) and observed (+) XRD patterns for the as cast  $TiMn_{1.5}$  powder. The discrepancy between the refined and observed patterns is shown at the bottom of the figure.

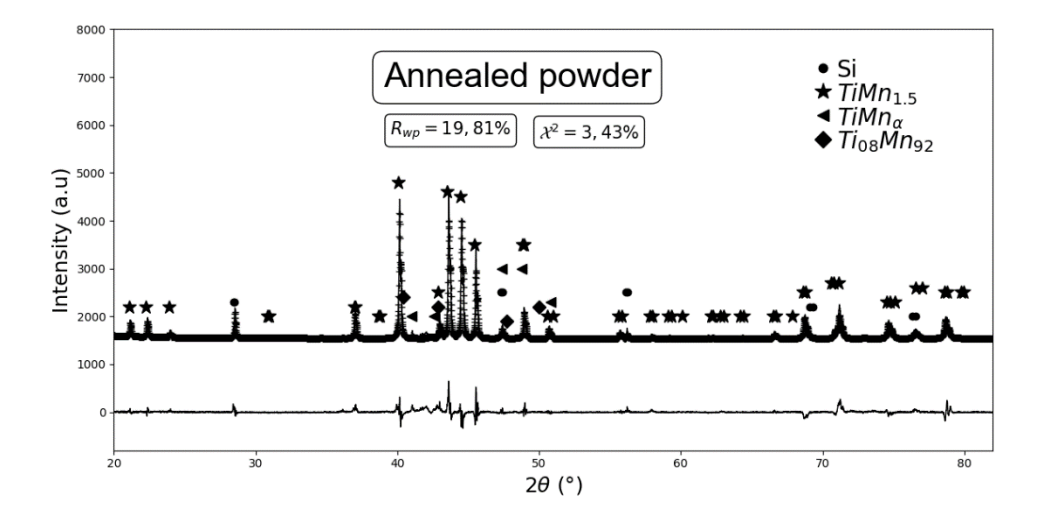


**Figure 7.** Rietveld refinement (line) and observed (+) XRD patterns for the annealed TiMn<sub>1.5</sub> powder. The discrepancy between the refined and observed patterns is shown at the bottom of the figure.

Experimental diffractogram identification by correlation with crystallographic database records confirm the presence of a Laves  $C_{14}$  structure phase. Nevertheless, additional diffraction peaks are noticeable more specifically between 40°- 43° and 72°-74°. These diffraction peaks come from presence of secondary phases identified as  $TiMn_{\alpha}$  and  $Ti_{08}Mn_{92}$ . Phases quantity determined by Rietveld Refinement are shown in **Table 2** with their measurement uncertainties. It appears that the quantity of  $TiMn_{\alpha}$  is increasing with heat treatment.

Phases quantity	As cast powder	Annealed powder	
C14 Laves Phase (Wt %)	$94.93 \pm 0.27$	$92.90 \pm 8.40$	
TiMn (Wt %)	$1.07 \pm 0.09$	$4.77 \pm 0.49$	
Ti08Mn92 (Wt %)	$4.00 \pm 0.15$	$2.30 \pm 9.37$	

**Table 2.** Phase quantity determined by Rietveld Refinement.

	Theoretical lattice parameter		Lattice parameters of the as cast powder		Lattice parameters of the annealed powder	
Silicon	a = b = c = 5,4309  Å [14]		a = b = c = 5,4306  Å		a = b = c = 5,4309  Å	
C14 Laves Phase	a = 4,862 Å [15]	c = 7,969 Å [15]	a = 4,8640 Å	c=7,9763 Å	a = 4,8665 Å	c=7,9767 Å
lattice strain (u.a)			$0.00203 \pm 0.00045$ $0.00083 \pm 0.00023$		0.00023	

**Table 3.** Lattice parameters of the silicon and the Laves Phase structure and lattice strain identified by Rietveld Refinement for the as cast and annealed powder.

**Table 3** shows the lattice parameters of silicon, as cast powder and annealed powder. The lattice parameter of silicon, which serves as a calibration reference, is well identified and consistent with the theoretical one. The lattice parameters of the C14 structure are also consistent with the theoretical parameters while a and c are being experimentally slightly higher. Comparison of the as cast and treated powders spectra, in **Figure 6** and **Figure 7**, reveals no significant (20) angle change.

A complementary study on the  $TiMn_{1.5}$  microstrain is performed by Rietveld Refinement, (**Figure 6** and **Figure 7**). Analyses are only focused on the  $C_{14}$  structure because of its predominant presence and the major impact on hydrogen capacity absorption. The last line of **Table 3** indicates a decrease in residual stress after the annealing treatment, *ie* relaxation phenomenon. The lattice strain of the material is an indicator of the crystal structure disorder. This means that the atomic mobility increases during the annealing and allows a reorganization of the crystalline network.

This can be linked to the absorption/desorption properties enhanced by heat treatment. Indeed, interstitial sites of the C14 Laves phase favoring reversible interactions with hydrogen atoms and

formation of the hydride, conferring to these phases' good hydrogen storage capabilities [13]. Conversely, in highly deformed and constrained materials, the regular arrangement of atoms is thwarted. This observation, characterized physically by an increase in the density of dislocations, penalizes the circulation of hydrogen atoms and the stability of interstitial sites [16], [17]. Which directly results in the decrease of the absorption capacities. The disorder generated within the crystalline lattices leads to a decrease of the interstitial sites favorable to the absorption phenomenon. The increase in dislocation density is generated as soon as the casting is rapidly cooled on the copper mold and then during the grinding steps to obtain a powder [2]. Our raw material is thus highly strained and exhibits a distorted crystal lattice. We therefore suggest that a relaxation of the stresses provides a partial justification for the increase in hydrogen uptake mass capacity, but also for the flattening of the phase transformation plateau.

## Microstructural modifications.

According to Fruchart *et al.* [13], manganese atoms located in positions 2a and 6h of the C14 Laves TiMn<sub>2</sub> lattice can be substituted by titanium atoms. This substitution is possible because the properties and size of these atoms are very similar. In addition, Gamo's study [6] shows that the composition of the Laves C14 phase can vary between TiMn<sub>1.25</sub> and TiMn<sub>2</sub>, causing the lattice parameters variations according to Vegard's Law [18]. However, diffraction analyses highlight the invariance of the crystallographic structure of the sample with lattice parameters for the as-cast and annealed powder close to the theoretical one (**Table 3**). This implies that the TiMn<sub>1.5</sub> phase has the same atomic composition before and after annealing. Nevertheless, Statistical analysis of the areas occupied by TiMn<sub> $\alpha$ </sub> in the micrographs (**Figure 5**) clearly indicates the TiMn<sub> $\alpha$ </sub> domains increasing after annealing. We therefore propose a phenomenon of atomic migration from TiMn<sub>1.5</sub> domains to TiMn<sub> $\alpha$ </sub> domains at the interface, leading to an increase in the amount of TiMn<sub> $\alpha$ </sub>.

According to Gamo *et al.* [6], TiMn based alloys with more than 36% at. of Ti, are highly reactive during the hydridation and then have poor storage properties. We previously demonstrate that, the TiMn $\alpha$  phase, usually known with poor properties of storage, is increased by the annealing process, while the macroscopic storage capacity of the powder still increases. Based on our results we propose two roles for the TiMn $\alpha$  phase in improving storage capacity. Firstly, the TiMn $\alpha$  can serve as a catalyst element due to its high hydrogen reactivity, which implies faster diffusion into the intermetallic alloy during the activation process. Secondly, the TiMn $\alpha$  phase plays an important role in the decrepitation phenomenon, which involves an increase of the active surface of H<sub>2</sub>.

## **CONCLUSION:**

In 1985, Gamo *et al* studied the hydrogen storage properties of several Ti-Mn based alloys powders [6]. It appears that the TiMn<sub>1.5</sub> give the best reversible storage capacity, with a theoretical hydride structure TiMn<sub>1.5</sub>H<sub>2.3</sub> leading to a storage saturation at H/M≈0.92. Gamo *et al* suggested an annealing heat treatment of that drastically enhance the storage capacity and flatten the absorption/desorption plateaus. It doesn't clearly explain how such a heat treatment can modify storage reversible capacity to such an extent. Nevertheless, this treatment is still often applied indiscriminately to many metal hydrides, without formal knowledge of the underlying mechanisms.

In the present paper, we investigated effects of heat treatment on the material, prior to hydriding, using various experimental techniques so as to highlight changes that could explain significant improvement in hydrogen storage properties. We focused observations on powder grain morphology, microstructure and internal particle composition, with the aim of identifying which are the small-scale physico-chemical phenomena involved.

We have shown that annealing for 10h and 20h had exactly the same improvement effect (after treatment  $P_{abs} \approx 25$ bar  $P_{des} \approx 10$ bar at the center of the plateau, maximal storage is improved at 1.75 Hwt% @100bar). SEM micrographs have shown that the number of foamy particles with a "coral-like" aspect increases by 20% among faceted particles after treatment but no noticeable difference was reported within the core microstructure: both kind of particles presented two phases structure with 1 $\mu$ m thick elongated dark domains embedded in bright Mn richer matrix. EDS chemical analysis has shown that dark domains were TiMn $_{\alpha}$  embedded in a matrix with a composition close to 60% Mn plus 40% Ti that we identified as C14 Laves phase whose composition can varied between TiMn $_{1.5}$  or TiMn $_2$  in accordance with the model proposed by Singh *et al.* [7]

XRD analyses with Rietveld refinement revealed the presence of TiMn<sub>1.5</sub>, TiMnα and Ti<sub>08</sub>Mn<sub>92</sub>. Annealing leads to an unexpected increase of TiMnα phase while the amount of phase C14 and Ti<sub>08</sub>Mn<sub>92</sub> decreases. Heat treatment favors the mobility of Mn, dissolving the few pre-existing αMn known to be deleterious to hydrogen storage, enabling the enrichment of the C14 phase (up to TiMn<sub>1.7</sub>). XRD measurements did not indicate the lattice expansion expected according to Vegards' law. On the other hand, Rietveld refinement analysis has clearly shown that crystal distortions are recovered by annealing as part of a relaxation phenomenon, particularly in the Lave C14 phase, which is favorable to hydrogen storage in its interstitial sites. While these analyses are subject to major measurement uncertainties, this is fully consistent with the flattening of the transformation plateau of the PCI curves.

Ameliorative effect on the sorption properties of TiMn<sub>1.5</sub> powder is assumed to be the result of particle morphology changes, increasing the specific surface and creating entry points for H<sub>2</sub>, but above all the result of thermal activated residual stress relaxation. The role of Mn migration should

be the purpose of further investigation, because while it positively enriches the C14 phase, increasing the affinity to H of its interstitial sites, it also increases the amount of TiMn $\alpha$  phase, normally deleterious to H<sub>2</sub> storage. A credible hypothesis, but yet to be demonstrated, would be that this phase, which normally has a high but irreversible affinity with H, may act as a catalyst.

#### **AUTHOR INFORMATION**

# **Corresponding Author**

\*anne.maynadier@univ-fcomte.fr; anne.maynadier@femto-st.fr; https://orcid.org/0000-0001-6419-3284

## **Author Contributions**

The manuscript was written through contributions of all authors. All authors have given approval to the final version of the manuscript. Authors contributed equally.

# **Funding Sources**

This work has been supported by the EUR EIPHI Graduate school (contract "ANR-17-EURE-0002") and by the Bourgogne-Franche-Comté Region. This work was partly supported by the French RENATECH network and its FEMTO-ST technological facility "MIMENTO".

## **ACKNOWLEDGMENT**

We would like to thank Dr M. Raschetti (RENATECH, FEMTO ST Institute) for her expert technical assistance and interesting discussions on EDS analyses. We also would like to express our thanks to G. A. Campion and E. Louyot, ENSMM-Sup'Microtech students involved in the

sorption experiments. Authors thanks HENSOLD - MAHYTEC (Dôle, France) for the providing of synthetized storage material.

## **REFERENCES**

- [1] Aceves, S.M.; Espinosa-Loza, F.; Ledesma-Orozco, E.; Ross, T.O.; Weisberg, A.H.; Brunner, T.C.; Kircher, O. High-density automotive hydrogen storage with cryogenic capable pressure vessels. *Int. J. Hydrog. Energy.* **2010**, 35 (3), 1219-1226. DOI:10.1016/j.ijhydene.2009.11.069.
- [2] Zeaiter, A.H. Caractérisation et modélisation du comportement des alliages TiFe dédiés au stockage solide d'hydrogène. Application à l'amélioration des performances d'un réservoir à hydrures métalliques. Ph.D. Thesis, Université Bourgogne Franche-Comté, Besançon, France 2017. Français. (NNT: 2017UBFCD007). (tel-01810345)
- [3] Zheng,J.; Liu,X.; Xu, P.; Liu, P.; Zhao,Y.; Yang,J. Development of high pressure gaseous hydrogen storage technologies. *Int. J. Hydrog. Energy.* **2021**, 37 (1), 1048-1057, DOI: 10.1016/j.ijhydene.2011.02.125.
- [4] Volodin, A. A.; Denys, R.V.; Wan, C.; Dewi Wijayanti, I.; Suwarno, Tarasov, B. P.; Antonov, V. E.; Yartys, V. A. Study of hydrogen storage and electrochemical properties of AB2-type Ti0.15Zr0.85La0.03Ni1.2Mn0.7V0.12Fe0.12 alloy. *J. Alloys Compd.* **2019**, 793, 564-575, DOI: 10.1016/j.jallcom.2019.03.134.
- [5] Liang, G.; Huot, J.; Boily, S.; Van Neste, A.; Schulz, R. Hydrogen storage in mechanically milled Mg–LaNi5 and MgH2–LaNi5 composites. *J. Alloys Compd.* **2000**, 297 (1-2), 261-265, DOI: 10.1016/S0925-8388(99)00592-7.

- [6] Gamo, T.; Moriwaki, Y.; Yanagihara, N.; Yamashita, T.; Iwaki, T. Formation and properties of titanium-manganese alloy hydrides, *Int. J. Hydrog. Energy*, **1985**, 10 (1), 39-47. DOI: 10.1016/0360-3199(85)90134-X.
- [7] Singh, B. K.; Singh, A. K.; Imam, A. M.; Srivastava, O. N. On the structural characteristics and hydrogenation behaviour of TiMn1.5 hydrogen storage material. *Int. J. Hydrog. Energy.* **2001**, 26 (8), 817-821. DOI: 10.1016/S0360-3199(01)00012-X.
- [8] Khan, A. U.; Brož, P.; Premović, M.; Pavlů, J.; Vřeštál, J.; Yan, X.; Maccio, D.; Saccone, A.; Giester, G.; Rogl, P. The Ti–Mn system revisited: experimental investigation and thermodynamic modelling. *Phys. Chem. Chem. Phys.* **2016**, 18 (33), 23326-23339. DOI: 10.1039/C6CP04542A
- [9] Zhang, F.; Weidmann, A.; Nebe, J. B.; Beck, U.; Burkel, E. Preparation, microstructures, mechanical properties, and cytocompatibility of TiMn alloys for biomedical applications. *J. Biomed. Mater. Res. B Appl. Biomater.* **2010**, 94B (2), 406-413, DOI: 10.1002/jbm.b.31668.
- [10] Broz, P.; Rogl, G.; Yan, X.; Premović, M.; Soprunyuk, V.; Heinrich, P.; Bauer, E.; Schranz, W.; Rogl, P.; Physical properties of TiMn2 and interaction with refractory TiN (system Ti-Mn-N). *J. Alloys Compd.* **2018**, 740, 647-659. DOI: 10.1016/j.jallcom.2017.12.343.
- [11] Schneider, C. A.; Rasband, W. S.; Eliceiri, K. W. NIH Image to ImageJ: 25 years of image analysis. *Nature Methods*. **2012**, 9 (7), 671-675. DOI: 10.1038/nmeth.2089
- [12] Xinnan, Y.; Zhangda, L.; Surface study of Hydrogen storage material on TiMn1.5. Hydrogen Systems. International Symposium on Hydrogen Systems, 7–11 May 1985, Beijing, China. 1986, 431-436. DOI: 10.1016/B978-1-4832-8375-3.50047-3

- [13] Fruchart, D.; Soubeyroux, J. L.; Hempelmann, R. Neutron diffraction in Ti1.2,Mn1.8 deuteride: structural and magnetic aspects. *J. -Common Met.* **1984**, 99 (2), 307-319. DOI: 10.1016/0022-5088(84)90229-7
- [14] Elliot, A.D.; Structure of pyrrhotite 5*C* (Fe9S10), *Acta Crystallogr. Sect. B*, **2010**, 66 (3), 271-279. DOI: 10.1107/S0108768110011845.
- [15] Fruchart, D. ICSD:104990, ICSD Database Version 5.0.0. https://icsd.fiz-karlsruhe.de/search/basic.xhtml (accessed 2022-02-05)
- [16] Chêne, J. L'hydrogène dans les matériaux métalliques en relation avec les interactions plasticité-environnement, *PlastOx 2007*, **2009**, 131-145, DOI: 10.1051/ptox/2009010.
- [17] Oudriss, A. Influence des hétérogénéités métallurgiques sur les processus de diffusion et de piégeage de l'hydrogène dans le nickel, Ph.D. Thesis, Sciences des matériaux, Université de la Rochelle, La Rochelle, France, 2012. Français. (NNT: 2012LAROS383). (tel-00950603)
- [18] Fournet, G. Étude de la loi de Vegard, *J. Phys. Radium*, **1953**, 14 (6), 374-380. DOI: 10.1051/jphysrad:01953001406037400.

References are formatted in accordance with the *The ACS Style Guide*, available from Oxford Press as recommended <a href="https://doi.org/10.1021/acsguide.40303">https://doi.org/10.1021/acsguide.40303</a>